A Matrix-Isolation Spectroscopic and Theoretical Investigation of Tris(8-hydroxyquinolinato)aluminum(III) and Tris(4-methyl-8-hydroxyquinolinato)aluminum(III)†

Gary P. Kushto,*,‡ Yasuhiro Iizumi,§,|| Junji Kido,|| and Zakya H. Kafafi*,‡

United States Naval Research Laboratory, 4555 Overlook Avenue SW, Washington, D.C. 20375, and Graduate School of Engineering, Yamagata University, Yonezawa, Yamagata 992-8510, Japan

Received: November 2, 1999; In Final Form: February 2, 2000

Infrared and photoluminescence spectra of matrix-isolated and thin-film samples (both at 11 K) of tris(8-hydroxyquinolinato)aluminum(III) (Alq_3) and tris(4-methyl-8-hydroxyquinolinato)aluminum(III) ($Almq_3$) were collected and compared to vibrational spectra generated by B3LYP based density functional calculations. The present infrared spectral results suggest that both Alq_3 and $Almq_3$ exist primarily in the meridional or C_1 isomeric form with little or no spectral evidence for the presence of the alternate, facial (C_3 symmetry) geometric isomer. In addition, photoluminescence spectra of these molecules isolated in an argon matrix show vibronic structure in the emission band associated with the $S_1 \rightarrow S_0$ transition.

1. Introduction

Oxine metal complexes are well established in the analytical chemistry laboratory because of their unique fluorescence properties and have been used for the qualitative analysis of metal cations in solution for decades.[1−4] These bidentate ligands are well suited for analytical chemistry pursuits because the parent compound (oxine or 8-hydroxyquinolinol) exhibits very little fluorescence, but the 8-hydroxyquinolinato−metal complexes exhibit an intense photoluminescence signature. Since only the coordinated form of the oxine fluoresces, the intensity of the light emitted by an 8-hydroxyquinolinol/metal cation solution is directly proportional to the amount of metal in the sample, making qualitative analysis of the sample very straightforward. Although such systems are accurate and well established, the widespread use of more sensitive and easily automated spectroscopic techniques such as atomic absorption and atomic emission have caused fluorometric techniques to wane, and the 8-hydroxyquinolinato−metal complexes have found little favor among researching chemists. Interestingly, there has been one oxine complex that has recently come to the center of a firestorm of research interest, tris(8-hydroxyquinolinato)aluminum(III) or Alq_3.

In 1987, two scientists working at Kodak grew a bilayer nanostructure composed of ultrathin, vapor deposited layers of diamine and Alq_3 and found that when a voltage was applied across this structure it emitted light at very low driving voltages.[5] Although organic electroluminescence (EL) is not a new phenomenon, these devices exhibited remarkable efficiencies endowed them by the nature of the bilayer structure. By growing a layer of material that is primarily an electron transporter (Alq_3) on top of a layer that is primarily a hole transporter (diamine), an interface is formed that tends to build up a charge upon the application of an external potential. Since a high density of carriers builds up at this organic−organic interface, the probability of electron−hole recombination is significantly increased which in turn increases the EL efficiency. It was recognized immediately that the high EL efficiency of these molecular organic light emitting devices (MOLEDs) would make them ideal candidates for application as pixel elements in active-matrix flat panel displays. As a result, a tremendous amount of research has been devoted to the evaluation of every possible operational characteristic of these devices.[6−9]

With the introduction of several different hole transport materials and substantially more complex structures, these devices have undergone an evolution of sorts since the first report of their development; however, one element of their character has remained largely unchanged, and that is the extensive use of Alq_3 as the electron injection, electron transport and emitting layer material in these devices. More recently, the 4-methyl derivative of Alq_3, tris(4-methyl-8-hydroxyquinolinato)aluminum(III) ($Almq_3$),[10] has received attention as an alternative because it has significantly higher photoluminescence[11] and electroluminescence quantum yields.[12] Unlike Alq_3, $Almq_3$ has only been recently applied to the MOLED technology and has not received the intense scientific scrutiny that has been focused on the parent molecule. As such, $Almq_3$ is significantly less well characterized than Alq_3. Regardless, the importance of these metal complexes to the burgeoning MOLED industry has brought at least the parent compound under intense investigation by numerous groups.[6−9] The majority of these studies has been limited to the ultraviolet (UPS) and X-ray (XPS) photoelectron spectroscopy of Alq_3 because these techniques reveal important information about the energies of the molecular orbitals of this species and how they relate to the Fermi levels of different metal cathode materials.[13−17] Beyond the use of UPS and XPS, there have been few investigations that explicitly focus on the electronic and geometric structures of this molecular species.

Although Alq_3 has received significant attention from materials scientists and device physicists, there has been surprisingly little recent research activity associated with the molecule using more traditional chemical analysis tools, and there have been

† Part of the special issue "Marilyn Jacox Festschrift".

* To whom correspondence should be addressed. E-mail: kushto@nrl.navy.mil or kafafi@nrl.navy.mil.

‡ United States Naval Research Laboratory.

§ Current address: Fubata Corporation, 1080 Yabutsuka, Chousei, Chiba, 299-4395 Japan.

|| Yamagata University.

10.1021/jp993883t CCC: $19.00
Published on Web 03/30/2000

no such investigations for the 4-methyl derivative. The geometric structure of Alq_3 in a single crystal has been evaluated, and found that the meridional isomer of Alq_3 is the favored form; however, these structures included solvent molecules that formed strong hydrogen bonds with at least one of the oxygens in the complex.[18] An infrared and ab initio Hartree−Fock (calculations conducted only on the facial isomer) investigation of this species has also been conducted to provide assignments for the characteristic infrared peaks used by materials scientists in the analysis of Alq_3 films.[19] More recently, the IBM research group at Zurich has used density functional theory to model this complex in both the meridional and facial forms and as such were the first to conduct a complete theoretical investigation on both geometric isomers of Alq_3.[20−22] In these investigations, the latter group found that the meridional isomer is more thermodynamically stable, but under certain chemical conditions, the facial isomer can become the preferred form.[22] In addition, these studies found that the facial isomer may act as an electron trap if present in an amorphous film of Alq_3, suggesting that the latter form may govern charge transport in Alq_3 based devices. With this in mind, there has been no experimental attempt to evaluate the relative populations of the two possible geometric isomers of Alq_3 or $Almq_3$ under the conditions typical for device fabrication. For this reason, we have undertaken a matrix-isolation infrared spectral investigation of these molecular species.

By the very nature of the technique, the matrix-isolation method is well suited for this type of investigation. The common sample preparation methods shared between the typical MOLED preparation and the matrix-isolation experiment make it obvious that the latter technique is well suited to model chemical processes that occur during the MOLED vapor deposition process. In addition, once isolated in the cold argon matrix, molecular species experience very little interaction with their environment which tends to narrow spectroscopic bandwidth and hence deconvolutes what would be observed as an overlapping band structure when studied using a more conventional spectroscopic technique. When used in conjunction with quantum chemical calculations, matrix-isolation infrared spectroscopy has proven to be an indispensable tool in the characterization of molecular species. The information gleaned in this study will be used to determine what isomeric forms of Alq_3 and $Almq_3$ are predominant in the solid phase. These results may have a significant effect on the understanding of the charge transport and luminescent properties of these materials in the bulk.[22] Furthermore, the photoluminescence spectra of the matrix-isolated materials will be used to provide insights into the fluorescence emission from the first singlet excited states of both Alq_3 and $Almq_3$.

2. Experimental Details

The multiple-surface, matrix-isolation apparatus has been described in detail previously.[23,24] Briefly, the apparatus consists of a central copper block that is thermally linked via a cryolink (multiple copper foils) to a gold-plated copper wheel containing 15 spectroscopic substrates. This central copper block is mounted on the second stage of an APD (Allentown, PA) model CSW-202 closed-cycle helium refrigerator which allows the entire apparatus to be cooled to 11−12 K as measured by a Lakeshore Cryotronics (Westerville, OH) silicon diode−temperature controller (model DRC-84C) pair. The flexible copper foils facilitate the rotation of the cold substrates through a complete 360° turn without jeopardizing vacuum or thermal integrity.

The infrared spectrum of each sample was collected by reflectance−absorbance infrared spectroscopy (RAIRS) using a Nicolet 740 FTIR spectrometer (Madison, WI) with a liquid nitrogen cooled MCT-B detector. Photoluminescence spectra were collected by a SPEX (Instruments SA, Metuchen, NJ) 270M monochromator (0.27 m light path length) outfitted with a liquid nitrogen cooled CCD detector (Oriel, Stratford, CT). The excitation for the photoluminescence spectra was provided by the 325 nm line of an Omnichrome model 100 HeCd laser (Chino, CA).

The substances used in this investigation, tris(8-hydroxyquinolinato)aluminum(III) (Alq_3) and tris(4-methyl-8-hydroxyquinolinato)aluminum(III) ($Almq_3$),[10] were purified by train sublimating each material twice before use. Solid matrices containing the Alq_3 and $Almq_3$ were prepared by co-depositing the vapor phase molecular materials (which were evaporated from resistively heated Pyrex cells) with an excess of argon gas (Matheson, 99.9995%) onto the cold spectroscopic substrates. Relative rates of deposition and hence Ar/analyte mole ratios were determined using a quartz crystal microbalance which was mounted directly on the cold sample wheel. The composition of the matrices was varied between 20/1 and 10000/1 (Ar/analyte) in order to evaluate the effects of the guest concentration on both the infrared and PL spectra of the matrix sample. Each sample was the result of between 30 min and 2 h of co-deposition with the total time being governed by the acceptability of the signal-to-noise ratio in the resultant IR spectra.

3. Computational Methods

All of the included calculations were performed using the *Gaussian 98* suite of programs.[25] This software system was compiled for parallel processing on the 256 node IBM SP2 located at the Wright-Patterson Air Force Base Aeronautical Systems Center/Major Shared Resource Center. The geometry optimizations and vibrational frequency calculations presented herein were carried out using the three-parameter hybrid density functional of Becke[26] with additional local and nonlocal correlation corrections attributable to Lee, Yang, and Parr[27] (B3LYP). The electronic shell structure of each atom was described using the double ζ quality basis sets, and associated effective core potentials (ECPs) of the Stuttgart/Dresden group (SDD) as are included in the internal basis set library of the *Gaussian 98* suite.[28,29] In this set, the hydrogen atoms are characterized by the typical all-electron D95V basis,[30] while the heavy atoms (C, N, O, Al) each have their 1s shells frozen by the nodeless ECP and the valence electrons described by an optimized double ζ quality Gaussian basis.

4. Results

The aluminum tris-chelate complexes Alq_3 and $Almq_3$, whose structures are presented pictorially in Figure 1, have been investigated using matrix-isolation infrared spectroscopy in conjunction with hybrid density functional theory in an attempt to elucidate both the vibrational spectra of these important species as well as to provide insights into the conformational structures that these complexes take in the solid state. The accuracy of the present calculations has been verified by comparing selected molecular properties (primarily metal−ligand bond lengths) determined herein with those calculated previously[21,22] as well as those determined from X-ray crystallography.[18] These data are presented for the C_1 and C_3 symmetry isomers in Table 1. The infrared spectra in the 1700−450 cm^{-1} region of Alq_3 and $Almq_3$ isolated in solid argon and those

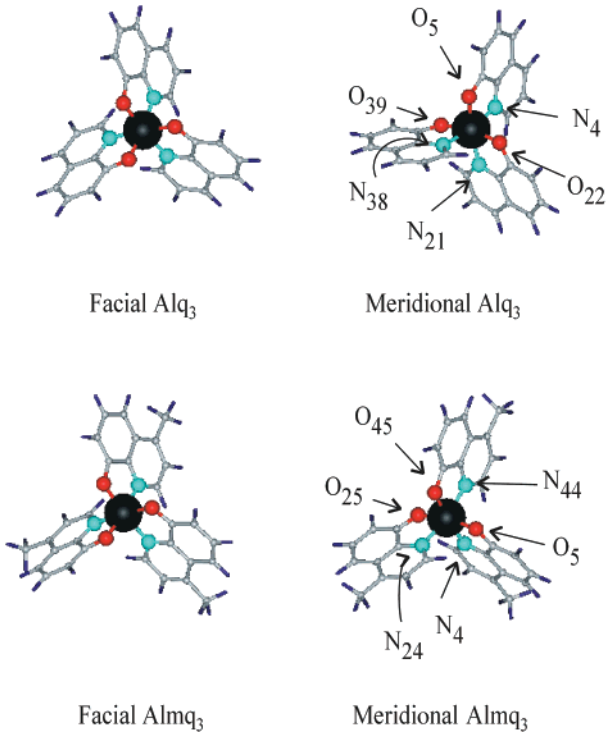

Figure 1. B3LYP/SDD calculated structures of tris(8-hydroxyquinolinato)aluminum(III) and tris(4-methyl-8-hydroxyquinolinato)aluminum-(III). Note that the relative diameters of the oxygen, nitrogen and aluminum atoms have been increased with respect to the carbon and hydrogen atoms to emphasize the symmetry of the local coordination sphere of the aluminum cation in each complex.

TABLE 1: Comparison of the Al−O and Al−N Bond Lengths (Å) Resultant from the Current Investigations with Those from Previous DFT and Hartree−Fock Analyses and X-ray Crystallographic Analysis of the Meridional Isomer

facial isomer	B3LYP/SDD[a]	BLYP/ECP[b]	HF/6-31G*[c]
Al−N	2.132	2.147	2.182
Al−O	1.882	1.852	1.816
meridional isomer	**B3LYP/SDD[a]**	**BLYP/ECP[b]**	**X-ray data[d]**
$Al-N_4$	2.084	2.089	2.048
$Al-N_{21}$	2.056	2.073	2.026
$Al-N_{38}$	2.114	2.151	2.073
$Al-O_5$	1.885	1.860	1.841
$Al-O_{22}$	1.918	1.885	1.882
$Al-O_{39}$	1.915	1.880	1.841

[a] Current investigation. [b] Reference 21. [c] Reference 19. [d] Reference 18.

spectra simulated from the results of the B3LYP/SDD calculations are compared in Figures 2 and 3. In addition, the latter spectra are expanded (Figures 4 and 5, Alq_3 and $Almq_3$, respectively) to show the metal−ligand stretching regions (750−500 cm^{-1}) in greater detail. The observed vibrational frequencies and vibrational spectral assignments with reference to the computational results are presented in Tables 2 and 3 for Alq_3 and $Almq_3$, respectively.

Finally, an investigation of the excited states of both aluminum complexes has been effected with the photoluminescence spectra of both Alq_3 and $Almq_3$ isolated in a solid argon matrix. These spectra are depicted in Figure 6 with associated spectral frequencies presented in Table 4.

5. Discussion

5.1. Computational Results. This section focuses on the structural and energetic aspects of Alq_3 and $Almq_3$ based on the present B3LYP/SDD calculations and compares these results to those presented in previous reports. Central to the current investigation are the relative energetics of the two isomeric forms of both Alq_3 and $Almq_3$ which can be readily evaluated using quantum theory. The geometric configurations of the Alq_3 and the $Almq_3$ species are typified by a central aluminum atom (in a +3 formal oxidation state) which is surrounded in a "pseudo-octahedral" environment by the three quinolate ligands. A pictorial representation of the optimized B3LYP/SDD structures of both Alq_3 and $Almq_3$ is presented in Figure 1. Each complex can occur in two isomeric forms, namely a facial isomer in which the oxygen and nitrogen atoms of the coordinating quinolate ligands share opposite faces of the octahedral complex and a meridional form in which the latter atoms lie along opposing edges of the octahedron. The ab initio calculations carried out by the IBM Zurich group have provided to date the most complete model of the electronic structures of both isomers of Alq_3. By applying pure density functional theory to this system, they predicted that the meridional isomer is more stable than the facial form.[21] In addition, Halls and Aroca utilized basic Hartree−Fock theory to produce an optimized geometry and harmonic vibrational frequencies for the facial isomer of Alq_3.[19]

As with the previous DFT investigations of the two Alq_3 isomers, the current B3LYP results predict that the meridional isomer is energetically more stable than the facial isomer. The initial work by Andreoni and co-workers indicates that at the BLYP level of theory the meridional isomer is energetically favored by as little as 4 kcal/mol, while the current investigation finds that the meridional structure is more stable by 7.8 kcal/mol, a difference that increases to 8.0 kcal/mol with the inclusion of the ZPE correction. Typically, the hybrid functional used in the current investigation provides more reliable energies than the pure DFT functional used in the previous study, suggesting a deeper potential for the meridional isomer; however, differences in the basis set quality used in the two studies may account for some portion of this difference. Table 1 compares the results for the Al−N and Al−O distances calculated in this work with those from the previous DFT studies,[21,22] the HF study of Halls and Aroca[19] (for the facial isomer), and the X-ray crystallographic data collected by Schmidbaur et al. on the meridional isomer.[18] It can be seen that the average difference between the B3LYP and BLYP results for the Al−N and Al−O bond lengths is 0.02 Å and 0.03 Å, respectively, for both isomers. The HF results for the facial isomer of Alq_3 underestimate the Al−O bond lengths and overestimate Al−N bond lengths relative to those determined using the DFT-based methods. Comparison of the B3LYP and BLYP bond lengths of the meridional isomer of Alq_3 with those derived experimentally from X-ray crystallography (see Table 1) supports the accuracy of these methods for the prediction of structural properties.

The meridional $Almq_3$ isomer is found to be 7.8 kcal/mol (with the inclusion of the ZPE correction) more stable than the associated facial isomer. In this species, the Al−N and Al−O bond lengths are found to be nearly identical (to within 0.005 Å) to those of the Alq_3 complexes calculated at the same level of theory.

5.2. Conformational Analysis of Alq_3 and $Almq_3$ Based on Argon Matrix Infrared Spectra and B3LYP/SDD Calculations. The isomers of Alq_3 and $Almq_3$ belong to two separate point group symmetries and as such should be spectroscopically identifiable by means of a thorough vibrational analysis. The facial isomer (referred to as fac-Alq_3 or fac-$Almq_3$) belongs to the C_3 point group while the meridional isomer (mer-

TABLE 2: Argon Matrix Observed and B3LYP/SDD Harmonic Calculated Vibrational Frequencies (cm^{-1}) for Tris(8-hydroxyquinolinato)aluminum(III) (Alq_3)

Ar matrix[a]	C_1 isomer (B3LYP/SDD)	C_3 isomer (B3LYP/SDD)	mode description	Ar matrix[a]	C_1 isomer (B3LYP/SDD)	C_3 isomer (B3LYP/SDD)	mode description
	3263 (4)[b]	3257 (15) a[c]	C−H str.		1004 (0)	976 (1) a	C−H op wag
	3262 (3)	3256 (6) e	C−H str.		998 (0)	969 (3) e	C−H op wag
	3260 (10)		C−H str.		972 (2)		C−H op wag
3075 w/br.	3246 (13)	3249 (6) e	C−H str.		945 (0)	940 (0) a	C−H,C−N,Al−N str/CCC def.
	3245 (11)		C−H str.		940 (3)	937 (2) e	C−H,C−N,Al−N str/CCC def.
	3242 (12)	3249 (18) a	C−H str.		936 (2)		C−H,C−N,Al−N str/CCC def.
	3240 (17)	3237 (16) a	C−H str.		908 (1)	906 (4) e	C−H op wag
	3239 (15)	3236 (13) e	C−H str.		905 (1)		C−H op wag
	3237 (16)		C−H str.	863 vw/br.	901 (2)	906 (1) a	C−H op wag
	3225 (28)	3225 (50) e	C−H str.	827.6	857 (83)	850 (70) a	C−H op wag
3058 br.	3224 (43)		C−H str.	825.8	854 (64)	849 (63) e	C−H op wag
	3224 (30)	3225 (0) a	C−H str.	823.6	848 (64)		C−H op wag
3048 w/br.	3211 (6)	3211 (5) e	C−H str.		837 (26)	835 (20) e	CCC def.
	3210 (11)		C−H str.		835 (6)		CCC def.
	3210 (1)	3211 (4) a	C−H str.	807.5	835 (29)	835 (21) a	CCC def.
	3204 (8)	3205 (10) e	C−H str.	792.0	806 (20)	806 (10) a	CCCC tors.
	3203 (10)		C−H str.		806 (12)	804 (22) e	CCCC tors.
	3203 (10)	3205 (9) a	C−H str.	786.4	803 (23)		CCCC tors.
1611 sh	1654 (28)	1654 (0) a	C−C str.	759.7	780 (59)	778 (31) a	C−H op wag
1608.2	1654 (90)	1651 (113) e	C−C str.		779 (49)	778 (44) e	C−H op wag
	1651 (77)		C−C str.		777 (37)		C−H op wag
	1637 (0)	1633 (1) a	C−C str.	752.7	768 (21)	764 (0) a	Ring Breath/Al−N str.
	1635 (0)	1632 (1) e	C−C str.	755.1	767 (166)	764 (151) e	Ring Breath/Al−N str.
	1634 (0)		C−C str.	744.1	763 (109)		Ring Breath/Al−N str.
	1621 (31)	1617 (82) e	C−C str.	659 br.	669 (22)	667 (2) a	C−H op wag/CCCC tors.
1585.7	1621 (68)		C−C str.		666 (15)	666 (21) e	C−H op wag/CCCC tors.
1580.9	1612 (79)	1615 (0) a	C−C str.		665 (9)		C−H op wag/CCCC tors.
	1551 (12)	1550 (1) a	C−C str./C−H bend	650 sh.	655 (45)	650 (18) a	Al−O,Al−N str./CCC def.
1502.9	1549 (128)	1549 (90) e	C−C str./C−H bend	651.9	650 (61)	650 (59) e	Al−O,Al−N str./CCC def.
	1548 (108)		C−C str./C−H bend		635 (2)		Al−O,Al−N str./CCC def.
1482.0	1513 (58)	1513 (30) a	C−C,C−N str./C−H bend		616 (0)	615 (3) a	CCCC tors.
1476.8	1509 (246)	1506 (264) e	C−C,C−N str./C−H bend		614 (0)	614 (0) e	CCCC tors.
1472.4	1503 (228)		C−C,C−N str./C−H bend		614 (1)		CCCC tors.
	1487 (4)	1486 (4) e	C−H bend	578 vw/br.	589 (10)	587 (13) e	CCC def./Al−N,Al−O str.
1430.4	1486 (4)		C−H bend		587 (6)		CCC def./Al−N,Al−O str.
	1484 (4)	1485 (2) a	C−H bend		587 (10)	586 (5) a	CCC def./Al−N,Al−O str.
1397 sh.	1440 (28)	1432 (39) a	C−C,C−N str./C−H bend	551.3	561 (106)	560 (107) e	Al−O str./CCC def
	1437 (13)	1431 (26) e	C−C,C−N str./C−H bend	548.0	555 (130)		Al−O str./CCC def
	1434 (24)		C−C,C−N str./C−H bend	524.7	530 (23)	542 (4) a	Al−O str./CCC def
1391.1	1425 (142)	1424 (196) a	C−C,C−N str./C−H bend		523 (7)	519 (1) a	CCC def.
	1422 (152)	1421 (87) e	C−C,C−N str./C−H bend		520 (1)	517 (10) e	CCC def.
1384.1	1419 (94)		C−C,C−N str./C−H bend		519 (10)		CCC def.
1339.0	1380 (31)	1383 (9) a	C−C,C−N,CO str./C−H bend		499 (12)	495 (9) e	CCCC tors.
1329.9	1377 (92)	1376 (145) e	C−C,C−N,CO str./C−H bend		496 (10)		CCCC tors.
1335.2	1374 (163)		C−C,C−N,CO str./C−H bend		494 (1)	493 (0) a	CCCC tors.
	1327 (30)	1330 (0) a	C−O, C−C str.		485 (14)	483 (14) e	CCCC tors.
	1322 (95)	1326 (85) e	C−O, C−C str.	460.1	484 (21)		CCCC tors.
1286 br.	1319 (104)		C−O, C−C str.		473 (10)	474 (0) a	CCCC tors.
1243.1	1278 (16)	1277 (1) a	C−C str./C−H bend		435 (87)	437 (64) e	Al−N str./CCC def./Al−O bend
	1278 (14)	1275 (8) e	C−C str./C−H bend		433 (98)		Al−N str./CCC def./Al−O bend
	1274 (6)		C−C str./C−H bend		423 (34)	419 (26) a	Al−N str./CCC def./Al−O bend
	1267 (1)	1268 (4) a	C−C,C−N str./C−H bend		415 (6)	406 (20) e	Al−N str./CCC def.
1232.9	1266 (36)	1264 (26) e	C−C,C−N str./C−H bend		407 (2)		Al−N str./CCC def.
1231.2	1264 (36)		C−C,C−N str./C−H bend		369 (23)	349 (16) a	Al−N str./CCC def.
	1230 (1)	1231 (2) a	C−H bend		312 (3)	297 (0) a	CCCC tors.
	1230 (2)	1230 (2) e	C−H bend		291 (1)	294 (2) e	CCCC tors.
	1229 (0)		C−H bend		285 (0)		CCCC tors.
	1194 (2)	1193 (1) a	C−H bend		228 (0)	231 (0) a	CCCC tors.
	1193 (0)	1192 (0) e	C−H bend		222 (3)	223 (5) e	CCCC tors.
	1193 (0)		C−H bend		215 (7)		CCCC tors.
	1150 (32)	1150 (18) a	C−H bend		209 (0)	200 (4) a	CCCC tors./butterfly
1119.2	1146 (160)	1146 (135) e	C−H bend		201 (8)	189 (10) e	CCCC tors./butterfly
1117.6	1145 (150)		C−H bend		191 (10)		CCCC tors./butterfly
	1096 (4)	1095 (0) a	C−C str/CCC def./C−H bend		188 (4)	175 (1) a	CCCC tors./butterfly
1053 w/br.	1091 (13)	1094 (6) e	C−C str/CCC def./C−H bend		167 (0)	163 (1) e	CCCC tors./butterfly
	1089 (5)		C−C str/CCC def./C−H bend		158 (0)		CCCC tors./butterfly
1036.6	1071 (9)	1070 (5) e	C−C str/CCC def.		155 (1)	142 (0) e	CCCC tors./butterfly
	1066 (7)		C−C str/CCC def.		143 (1)		CCCC tors./butterfly
1032.1	1064 (17)	1069 (10) a	C−C str/CCC def.		138 (0)	135 (0) a	CCCC tors./butterfly
	1035 (1)	1026 (1) a	C−H op wag		53 (1)	55 (1) a	Al−O,Al−N def.
	1032 (1)	1025 (1) e	C−H op wag		49 (1)	47 (0) e	Al−O,Al−N def.
	1024 (1)		C−H op wag		45 (2)		Al−O,Al−N def.
	1008 (0)	1007 (0) e	C−H op wag		42 (1)	45 (1) a	Al−O,Al−N def.
	1005 (0)		C−H op wag		26 (1)	26 (1) e	Al−O,Al−N def.
	1004 (0)	1007 (0) a	C−H op wag		26 (0)		Al−O,Al−N def.

[a] Correlation between theoretically predicted and experimentally observed vibrational frequencies are approximate and should not be considered unambiguous spectral assignments. [b] Numbers in parentheses denote calculated spectral intensities expressed in km mol^{-1}. Intensities associated with modes of *e* symmetry do not account for the degeneracy. [c] Trailing letters denote the symmetry of the respective vibration. All vibrations are listed explicitly.

TABLE 3: Argon Matrix Observed and B3LYP/SDD Harmonic Calculated Vibrational Frequencies (cm^{-1}) for Tris(4-methyl-8-hydroxyquinolinate)aluminum(III) ($Almq_3$)

Ar matrix[a]	C_1 isomer (B3LYP/SDD)	C_3 isomer (B3LYP/SDD)	mode description	Ar matrix[a]	C_1 isomer (B3LYP/SDD)	C_3 isomer (B3LYP/SDD)	mode description
	3259 (2)[b]	3253 (9)a[c]	C−H str.	1157.6	1206 (103)	1207 (14) a	C−C str./C−H bend
	3259 (1)	3252 (8) e	C−H str.		1206 (19)	1206 (60) e	C−C str./C−H bend
	3256 (10)		C−H str.		1205 (49)		C−C str./C−H bend
	3246 (15)	3249 (8) e	C−H str.		1151 (6)	1148 (9) e	C−C str./CCC def.
	3245 (14)		C−H str.	1099.3 w/br.	1148 (5)		C−C str./CCC def.
	3242 (16)	3249 (20) a	C−H str.		1144 (7)	1148 (0) a	C−C str./CCC def.
3075 br.	3235 (25)	3237 (1) a	C−H str.		1101 (4)	1101 (4) a	Me rock
	3235 (20)	3236 (33) e	C−H str.		1101 (4)	1101 (4) e	Me rock
	3234 (22)		C−H str.	1034.5	1101 (5)		Me rock
	3224 (13)	3222 (8) e	C−H str.		1095 (12)	1095 (1) a	C−H bend
2961 br.	3224 (15)		C−H str.		1093 (12)	1094 (17) e	C−H bend
	3222 (13)	3222 (20) a	C−H str.	1058.2	1092 (13)		C−H bend
	3204 (15)	3205 (22) e	C−H str.		1059 (15)	1059 (6) a	Me rock
2987 br.	3203 (20)		C−H str.		1058 (5)	1058 (12) e	Me rock
	3203 (19)	3205 (12) a	C−H str.	1014.8	1057 (17)		Me rock
	3142 (19)	3141 (11) e	Me C−H str.		1020 (1)	1004 (0) e	C−H op wag
	3141 (20)		Me C−H str.		1014 (0)		C−H op wag
2931 br.	3140 (20)	3141 (38) a	Me C−H str.		1004 (0)	1004 (0) a	C−H op wag
2900 br.	3103 (13)	3104 (11) a	Me C−H str.		1001 (0)	991 (0) a	C−H op wag
	3103 (13)	3104 (12) e	Me C−H str.		1001 (0)	985 (1) e	C−H op wag
	3103 (12)		Me C−H str.		988 (1)		C−H op wag
	3044 (20)	3044 (28) e	Me C−H str.	944.1	962 (26)	963 (3) a	CCC def.
2862 br.	3043 (28)		Me C−H str.		958 (18)	959 (29) e	CCC def.
	3043 (22)	3044 (13) a	Me C−H str.	935.3	956 (22)		CCC def.
	1651 (48)	1651 (2) a	C−C str.	895.0	917 (70)	910 (3) a	CCC def./Al−N str.
1605.2	1650 (73)	1648 (109) e	C−C str.		915 (33)	909 (52) e	CCC def./Al−N str.
1597.1	1647 (72)		C−C str.	889.4	909 (41)		CCC def./Al−N str.
	1640 (17)	1636 (25) e	C−C str.		904 (5)	903 (7) e	C−H op wag
	1638 (15)		C−C str.	859.6	902 (5)		C−H op wag
	1637 (14)	1636 (5) a	C−C str.		899 (5)	903 (3) a	C−H op wag
	1612 (27)	1607 (51) e	C−C,C−N str.	840 br.	886 (32)	872 (32) a	C−H op wag
1579.9	1612 (40)		C−C,C−N str.		881 (30)	868 (23) e	C−H op wag
1574.0	1603 (55)	1604 (0) a	C−C,C−N str.	830.4	868 (28)		C−H op wag
	1559 (39)	1560 (20) a	C−C str./C−H bend	806.3	835 (59)	834 (31) e	CCC def.
	1556 (137)	1558 (142) e	C−C str./C−H bend		34 (5)		CCC def.
1510.5	1556 (203)		C−C str./C−H bend		834 (30)	834 (19) a	CCC def.
	1537 (11)	1536 (10) a	Me C−H def.		820 (6)	820 (5) e	C−H op wag/CCCC tors.
	1537 (11)	1536 (13) e	Me C−H def.		820 (5)		C−H op wag/CCCC tors.
	1536 (13)		Me C−H def.	816.7 vw	818 (7)	820 (13) a	C−H op wag/CCCC tors.
	1525 (11)	1523 (12) e	Me C−H def.	744.0	778 (90)	777 (73) e	C−H op wag
	1524 (12)		Me C−H def.	748 sh.	777 (62)		C−H op wag
	1524 (11)	1523 (10) a	Me C−H def.		775 (59)	776 (48) a	C−H op wag
1481.3	1514 (59)	1515 (47) a	C−C str./C−H bend	711.0	706 (107)	707 (161) e	Al−O str.
1474 sh.	1510 (285)	1507 (304) e	C−C str./C−H bend	705.8	700 (130)		Al−O str.
1469.1	1505 (285)		C−C str./C−H bend	692.9	694 (60)	705 (4) a	Al−O str.
	1465 (1)	1465 (0) e	Me umbrella		680 (5)	678 (5) a	CCCC tors.
	1465 (0)		Me umbrella		678 (5)	678 (5) e	CCCC tors.
	1465 (0)	1465 (0) a	Me umbrella		677 (2)		CCCC tors.
1417.3	1459 (42)	1459 (30) a	Me umbrella	620.2	648 (14)	646 (0) a	CCCC tors.
	1458 (23)	1459 (36) e	Me umbrella		646 (6)	645 (11) e	CCCC tors.
	1458 (37)		Me umbrella		644 (6)		CCCC tors.
	1439 (13)	1432 (16) a	C−N,C−C str.		612 (18)	608 (41) e	CCC def./C−O bend
	1436 (12)	1431 (12) e	C−N,C−C str.	609.7	608 (37)		CCC def./C−O bend
	1434 (9)		C−N,C−C str.	597.9	602 (5)	607 (12) a	CCC def./C−O bend
	1421 (68)	1420 (172) a	C−C str.	575.6	595 (6)	589 (5) a	ring breath/Al−N, Al−O str.
1388.4	1421 (164)	1418 (61) e	C−C str.	566.0	586 (14)		ring breath/Al−N, Al−O str.
1374.8	1418 (64)		C−C str.	545.6	559 (103)	556 (101) e	Al−O,Al−N str./CCC def.
1332 sh.	1370 (29)	1374 (23) a	C−H bend	542.8	557 (163)		Al−O,Al−N str./CCC def.
1324 sh.	1365 (118)	1366 (168) e	C−H bend	526.2	538 (14)	542 (0) a	Al−O,Al−N str./CCC def.
1321.5	1363 (201)		C−H bend	506.8	528 (6)	526 (11) e	CCCC tors.
1281.2	1330 (36)	1333 (0) a	C−C str./C−H bend	505.5	526 (11)		CCCC tors.
	1324 (74)	1329 (77) e	C−C str./C−H bend	501.1	522 (7)	521 (2) a	CCCC tors.
1290.1	1321 (95)		C−C str./C−H bend		505 (1)	501 (2) e	CCC def.
1250.7	1290 (30)	1289 (3) a	C-Me, C−C str./CCC def.		502 (1)		CCC def.
1246.2	1287 (35)	1288 (28) e	C-Me, C−C str./CCC def.		500 (6)	501 (1) a	CCC def.
	1285 (26)		C-Me, C−C str./CCC def.		493 (0)	492 (1) a	CCCC tors.
	1264 (1)	1265 (7) a	C−N,C−C str.		492 (0)	490 (0) e	CCCC tors.
1220.6	1262 (70)	1261 (45) e	C−N,C−C str.		490 (0)		CCCC tors.
	1259 (66)		C−N,C−C str.		460 (58)	461 (58) e	CCC def./Al−N str.
	1242 (1)	1243 (1) a	C−H bend/C−C str.		457 (32)		CCC def./Al−N str.
	1240 (2)	1240 (4) e	C−H bend/C−C str.	461 br.	452 (76)	454 (32) a	CCC def./Al−N str.
1194.6 w	1239 (4)		C−H bend/C−C str.		440 (50)	430 (54) e	Al−N str./CCC def.

TABLE 3 (Continued)

Ar matrix[a]	C_1 isomer (B3LYP/SDD)	C_3 isomer (B3LYP/SDD)	mode description	Ar matrix[a]	C_1 isomer (B3LYP/SDD)	C_3 isomer (B3LYP/SDD)	mode description
	434 (65)		Al−N str./CCC def.		169 (0)		CCCC tors./butterfly
	379 (23)	364 (13) a	Al−N str./CCC def.		161 (0)	156 (0) a	Me rotor
	327 (1)	325 (0) e	CCCC tors.		159 (0)	153 (1) e	Me rotor
	322 (2)		CCCC tors.		156 (0)		Me rotor
	309 (4)	311 (3) a	CCCC tors.		152 (1)	144 (0) a	Al−N str./C-Me op wag
	296 (4)	300 (1) a	C-Me op wag/CCCC tors.		144 (0)	142 (0) e	Al−N str./C-Me op wag
	289 (0)	289 (2) e	C-Me bend		129 (0)		Al−N str./C-Me op wag
	286 (0)		C-Me bend		120 (0)	118 (0) a	CCCC tors./C-Me op wag
	283 (3)	280 (2) a	C-Me bend		115 (0)	115 (0) e	CCCC tors./C-Me op wag
	275 (1)	272 (1) e	C-Me op wag/CCCC tors.		111 (0)		CCCC tors./C-Me op wag
	270 (1)		C-Me op wag/CCCC tors.		49 (1)	45 (0) a	Al−O,Al−N def.
	210 (7)	200 (15) e	CCCC tors./butterfly		41 (1)	40 (0) a	Al−O,Al−N def.
	206 (8)		CCCC tors./butterfly		38 (1)	40 (0) e	Al−O,Al−N def.
	197 (12)	199 (3) a	CCCC tors./butterfly		36 (1)		Al−O,Al−N def.
	190 (4)	181 (1) a	CCCC tors./butterfly		24 (1)	23 (1) e	Al−O,Al−N def.
	178 (0)	172 (1) e	CCCC tors./butterfly		22 (1)		Al−O,Al−N def.

[a] Correlation between theoretically predicted and experimentally observed vibrational frequencies are approximate and should not be considered unambiguous spectral assignments. [b] Numbers in parentheses denote calculated spectral intensities expressed in km/mol. Intensities associated with modes of *e* symmetry do not account for the degeneracy [c] Trailing letters denote the symmetry of the respective vibration. All vibrations are listed explicitly.

Alq_3 or mer-$Almq_3$) belongs to the C_1 point group. Although the forms of all of the vibrations in these complexes must conform to the point group symmetry of the whole, the modes directly associated with the metal−ligand bonds are expected to be of the simplest forms.

To simplify the vibrational analysis of each complex, one may consider an idealized form that contains just the atoms within the local coordination sphere of the aluminum atom, i.e., a complex having the stoichiometry AlN_3O_3. An analysis of the symmetry of such a complex reveals a C_{2v} local symmetry for the meridional isomer and a C_{3v} local symmetry in the facial isomeric form. In both conformations, there are expected to be six stretching coordinates, three Al−O modes and three Al−N modes. In the vibrational spectrum of the C_{3v} isomer, these modes will ideally appear as four separate absorptions, two due to the a_1 symmetry stretching modes of the Al−O and Al−N bonds and two due to the two sets of doubly degenerate stretching modes of *e* symmetry. In the lower symmetry conformer, the doubly degenerate modes of *e* symmetry found in the facial isomer each split into modes of a_1 and b_1 symmetry and hence the vibrational spectrum of this species should contain six distinct absorptions attributable to the Al−ligand stretches; however, it must be noted that the relative intensities and possibly small magnitudes of the mode splittings may preclude direct spectral observation.

With the above symmetry-based arguments in mind, characterization of the infrared spectrum of the matrix-isolated species should provide the information needed to evaluate the conformational distribution of Alq_3 and $Almq_3$ in the experimental reference sample. Unfortunately, the complexity of the infrared spectra presented in Figures 2 and 3 makes an evaluation of this sort very tricky business. The primary obstacle for a study of this nature is that the unambiguous identification of the Al−ligand stretching modes is only possible by way of isotopic labeling of the atoms involved in the vibrational modes of interest. Regrettably, aluminum has no other stable, naturally occurring isotopes, and isotopic labeling of the quinolate ligands would require an expensive synthesis. In an attempt to circumvent this problem, ab initio quantum chemical analyses of Alq_3 and $Almq_3$ have been completed and infrared spectra of each isomeric form have been simulated from the resultant theoretically derived harmonic force fields.

With the benefit of the calculations, the search for absorptions due to the metal−ligand vibrations can be narrowed to a reasonably small section of the vibrational spectra. The B3LYP/SDD calculations for the C_3 and C_1 isomers of Alq_3 predict that the Al−N stretching modes should occur at 349 (*a*) and 406 (*e*) for fac-Alq_3 and at 368, 432, and 435 cm^{-1} for mer-Alq_3. The expected low frequencies of the Al−N modes preclude direct observation in the current investigation (see Table 2); however, two previous vibrational analyses of the Alq_3

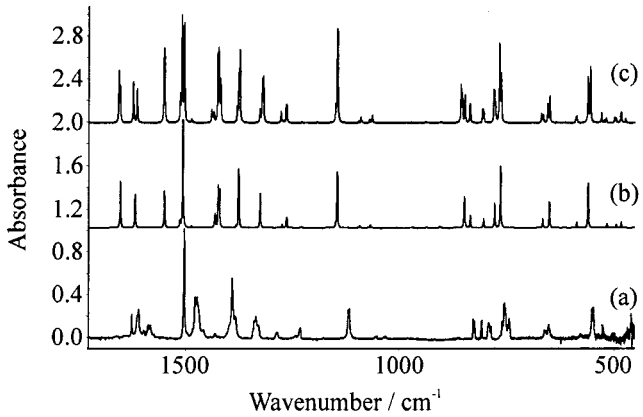

Figure 2. Comparison of the 1700−450 cm^{-1} regions of (a) the infrared specrum of Alq_3 in solid argon, (b) the B3LYP/SDD simulated infrared spectrum of fac-Alq_3, and (c) the B3LYP/SDD simulated infrared spectrum of mer-Alq_3.

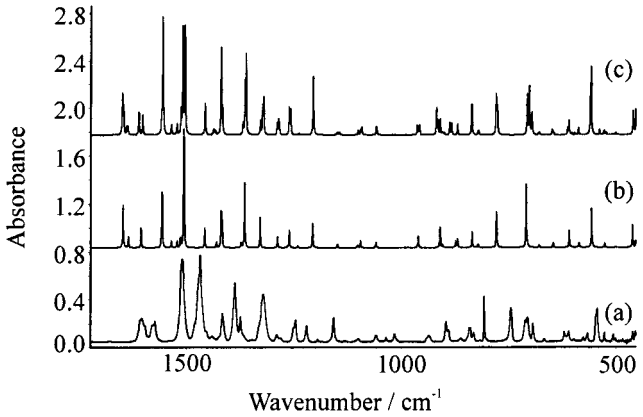

Figure 3. Comparison of the 1700−450 cm^{-1} regions of (a) the infrared spectrum of $Almq_3$ in solid argon, (b) the B3LYP/SDD simulated infrared spectrum of fac-$Almq_3$, and (c) the B3LYP/SDD simulated infrared spectrum of mer-$Almq_3$.

complex did address the low frequency region of the vibrational spectrum. The initial investigation was concerned strictly with the far-infrared spectra of several 8-hydroxyquinolinato−metal complexes in chloroform solution, and observed no bands below 355 cm^{-1} for Alq_3,[31] limiting the usefulness of this study to the current evaluation. A more recent vibrational investigation of Alq_3 assigned features at 315 cm^{-1} in the far-infrared and 314 cm^{-1} in the FT-Raman spectrum of a thin film sample to the symmetric Al−N stretch based on ab initio calculations conducted on the fac-Alq_3 isomer at the restricted Hartree−Fock level of theory.[19]

This investigation made no attempt to evaluate the vibrational spectrum of the meridional isomer and as such has neglected the possibility that the observed vibrational spectrum may be due to the lower symmetry conformer or a combination of the C_1 and C_3 isomers. The current DFT results make it clear that the mer-Alq_3 species will show a splitting in the antisymmetric Al−N stretching modes which matches well with the observed spectrum of Alq_3 dispersed in a KBr pellet (spectrum not shown). In this spectrum, an infrared absorption centered at 419.0 cm^{-1} shows unresolved multiplet structure and may be associated with the two antisymmetric Al−N stretching modes. Unfortunately, this feature appears in a region of the Alq_3 matrix spectra that has a very poor signal-to-noise ratio and as such is not discernible from the background. This feature was assigned as being due to ring deformation modes in the Halls and Aroca work.[19] The HF method is well known to significantly overestimate the vibrational force constants associated with bond stretching modes while exhibiting a somewhat smaller overestimation on the force constants associated with other modes such as valence bond bending coordinates.[32] This inconsistency is of little consequence in small molecules whose normal modes are well separated in energy; however, these errors are bound to severely effect the resultant forms of the calculated normal modes for a complicated system like Alq_3.

Close examination of the 700−500 cm^{-1} region of the matrix-isolation spectrum of Alq_3 (Figure 4) reveals two sets of medium intensity doublets that can be readily associated with the Al−O stretching coordinates of this complex. The B3LYP/SDD calculations suggest that the Al−O stretching internal coordinates play significant roles in two different sets of normal coordinates: one set at ≈650 and another at ≈550 cm^{-1} (see Table 2). These calculated spectral features match exceptionally well with the observed matrix infrared bands at 651.9 and 548.0−551.3 cm^{-1} (see Figure 4). Although the former band is somewhat broadened and unresolved, it is the clean resolution of the doublet features that provides strong support that the mer-Alq_3 isomer is the dominant form in the argon matrix. In addition, the relative intensities of the observed Al−O doublet at 548.0 and 551.3 cm^{-1} are nearly identical to those calculated, suggesting that little or no spectral contribution from absorptions due to fac-Alq_3.

The calculations suggest that in lowering the symmetry of the local coordination sphere of the Al^{3+} cation from C_{3v} to C_{2v}, the resulting Al−O stretching mode of b_1 symmetry will shift very little from its position as one of the doubly degenerate modes in the C_{3v} isomer. The other vibration has a_1 symmetry and can interact with the third, lower frequency Al−O stretching vibration because of their common symmetry. The effect of this interaction manifests itself two ways in the vibrational spectrum of the complex. First, the two modes of a_1 local symmetry are displaced from their energies in the C_{3v} local symmetry conformer with the higher frequency partner red shifting by ≈4 cm^{-1} from 560 to 555 cm^{-1} and the lower energy mode red shifting ≈12 cm^{-1} from 542 to 530 cm^{-1}. Second, the interaction of the two like-symmetry modes allows some "intensity stealing" to occur between the absorptions with the lower energy counterpart increasing significantly in intensity with respect to its cross section in the spectrum of the C_3 isomer (Figure 4). Comparison of the two simulated spectra with the observed matrix spectrum certainly supports the notion that the mer-Alq_3 isomer is governing the characteristics of the observed spectrum which suggests that fac-Alq_3 isomer is at the most a minor contributor to the spectral signature of the matrix; however, this does not prove that Alq_3 exists in only one isomeric form. It merely suggests that the meridional isomer is the majority form.

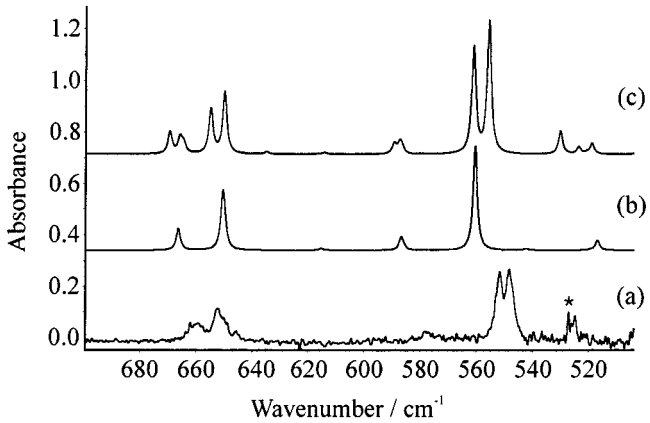

Figure 4. Comparison of the Al−O stretching regions (700−500 cm^{-1}) of (a) the infrared spectrum of Alq_3 in solid argon, (b) the B3LYP/SDD simulated infrared spectrum of fac-Alq_3, and (c) the B3LYP/SDD simulated infrared spectrum of mer-Alq_3. *Note: The sharp spike at 527.1 cm^{-1} is an electronic artifact and not due to the matrix sample.

The B3LYP/SDD calculations for $Almq_3$ in the facial isomeric form predict Al−N vibrations to occur at 364 (*a*) and 430 (*e*) cm^{-1} while in the meridional isomer, the Al−N stretching internal coordinates are found to play a significant role in the normal modes at 379, 457, and 459 cm^{-1}. No matrix spectra were collected in this study that would contain good data for absorptions that occur below 450 cm^{-1}; however, spectra of $Almq_3$ dispersed in a KBr pellet (spectrum not shown) contain a doublet of bands at 459 and 449 that can be assigned to the Al−N antisymmetric stretching modes of this complex. For more concrete evidence, the analysis of the Al−O stretching modes must be evaluated. In the matrix infrared spectrum of $Almq_3$, the triplet of bands that occurs at 711.1, 705.8, and 692.9 cm^{-1} and the intense, closely spaced doublet of bands at 545.6−542.8 cm^{-1} can both be attributed to Al−O stretching modes.

Investigation of Figure 5 shows the remarkable match between the mer-$Almq_3$ simulated and the observed $Almq_3$ matrix spectra which certainly suggests that the experimental sample contains primarily the meridional isomer of $Almq_3$. Once again, the intensities of these absorptions relative to one another and as compared to the simulated spectra suggest that if there is a contribution to this spectrum from the facial isomer it is small. Of particular note is the striking triplet of absorptions formed by the Al−O stretching vibrations of the $Almq_3$ complex at 711.0, 705.8, and 692.9 cm^{-1}. These features arise by the same splitting mechanism noted above for the mer-Alq_3 complex, except that in the methylated species, the coupling between the two normal modes of a_1 local symmetry is significantly stronger. In the fac-$Almq_3$ isomer, all three of the Al−O vibrations are nearly degenerate at 707 cm^{-1} with the two modes of *e* symmetry at 707 cm^{-1} and the associated a_1 mode occurring at 706 cm^{-1}. Because these vibrations lie so close in energy, when the local symmetry of the aluminum ion

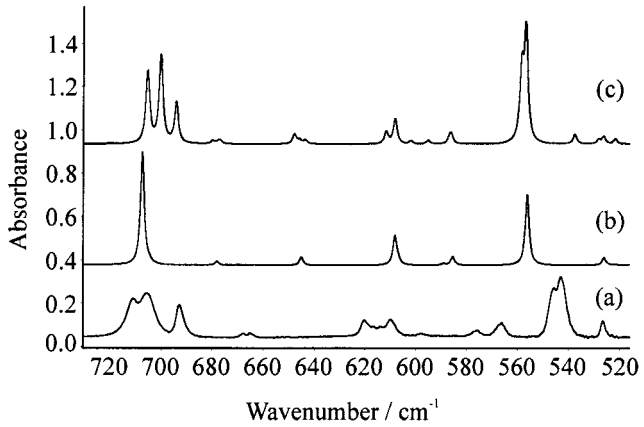

Figure 5. Comparison of the Al−O stetching regions (730−520 cm^{-1}) of (a) the infrared spectrum of $Almq_3$ in solid argon, (b) the B3LYP/SDD simulated infrared spectrum of fac-$Almq_3$, and (c) the B3LYP/SDD simulated infrared spectrum of mer-$Almq_3$.

is reduced to C_{2v}, the two produced modes of a_1 symmetry interact much more strongly and hence share intensities to a much greater extent to produce the features simulated at 700 and 694 cm^{-1} in the mer-$Almq_3$ spectrum. Conversely, the closely spaced doublet of bands observed at 545.6 and 542.8 cm^{-1} can be attributed to splittings that are more consistent with those observed for the analogous features in the Alq_3 example listed above. Regardless, the combination of these spectral effects and the fact that they are so well modeled by the B3LYP/SDD calculations provide ample support that $Almq_3$, like Alq_3, exists primarily in the meridional isomeric form.

5.3. Analysis of the Matrix Isolation Infrared Spectra of Alq_3 and $Almq_3$ with Emphasis on the Vibrations Localized in the Quinolate Ligands. As can be seen from Figures 2 and 3, the aluminum tris(8-hydroxyquinolinato)−metal complexes studied herein give rise to very rich and complicated infrared spectra, most of which can be attributed to the vibrations of the individual ligands themselves. Of the 150 vibrational modes associated with Alq_3 and the 177 vibrational modes associated with $Almq_3$, only fifteen in each complex are based on the Al−ligand bonds, and of these vibrations all but the Al−O stretching coordinates (six of these) are calculated as occurring below 500 cm^{-1}. It is obvious then that in order to fully characterize the infrared spectra of these complexes, the vibrations associated with the quinolate ligands should be considered in detail. The following discussion will outline the assignments of the matrix infrared spectra of both Alq_3 and $Almq_3$; however, because of the large nature of the problem, only the major spectral features will be discussed in detail with the smaller bands being assigned in Tables 2 and 3.

The most intense absorptions in the infrared spectra of the Alq_3 and $Almq_3$ complexes are directly attributable to the ring C−C stretching modes of the quinolate ligands. The bands in the matrix infrared spectra of Alq_3 (a doublet at 1611.0 and 1608.9 cm^{-1}, a doublet at 1585.7 and 1580.9 cm^{-1}, a single absorption at 1502.9 cm^{-1}, and a doublet at 1476.8 and 1472.4 cm^{-1}) are attributable to the skeletal stretching vibrations of the quinolate, fused ring system. As can be seen in Figure 2, these modes have been slightly overestimated by the B3LYP calculations with the associated spectral features occurring as a doublet at 1654 and 1651 cm^{-1}, a doublet at 1621 and 1613 cm^{-1}, a single absorption at 1549 cm^{-1}, and a doublet at 1509 and 1503 cm^{-1} in the simulated spectrum of mer-Alq_3.[33] It should be noted that all of the bands in this region except the sharp feature at 1502.9 cm^{-1} (1549 cm^{-1} simulated) occur as sets of doublets. Special attention should be brought to these splittings. In a manner comparable to the metal−ligand stretching modes discussed above, the other vibrational normal coordinates of these complexes also arise as effective linear combinations of the vibrations associated with the isolated 8-hydroxyquinoline ligands (or 4-methyl-8-hydroxyquinoline in the case of $Almq_3$). These normal modes can exhibit spectral splittings as a result of lowering symmetry in the complex; however, as can be seen with the absorption at 1502.9 cm^{-1}, the magnitude of this splitting may be very small.

Below 1400 cm^{-1}, the spectrum of Alq_3 is dominated by the aromatic C−H bending and wagging and benzenoid ring internal angle deformation modes. The intense multiplet feature at 1391.1−1384.1 in the matrix spectrum of Alq_3 can be assigned to the calculated triplet of vibrations at 1425, 1422, and 1419 cm^{-1} which are attributable to mixed modes that contain contributions from the asymmetric stretch of the C−N coordinates in the pyridyl side of the quinolate ligand as well as C−H in-plane bending motions. The medium intensity feature in the matrix spectrum that shows multiplet structure with maxima at 1339.0, 1335.2, and 1329.9 can be assigned to highly mixed modes that contain contributions from the in-plane motions of the rings as well as a significant contribution to each normal mode from the C−O stretching internal coordinate. The intense feature that appears as a closely spaced doublet, 1119.2−1117.6 cm^{-1}, can be associated with the closely spaced triplet of vibrations calculated at 1150, 1146, and 1145 cm^{-1} which are composed entirely of aromatic C−H in-plane bending coordinates.

The 800 cm^{-1} region is rich with a high density of absorptions. The triplet at 827.6, 825.8, and 823.6 cm^{-1} correspond primarily to out-of-plane ring vibrations with contributions from the aromatic C−H out-of-plane wagging and CCCC torsional motions of the quinolate skeleton. The multiplet feature with maxima at 759.7, 755.1, 752.7, and 744.1 cm^{-1} is also due to a sum of spectral features. The absorptions in this multiplet arise from the out-of-plane C−H wagging motions as well as in-plane deformations of the quinolate carbon skeleton coupled with the Al−N stretching coordinates. The lowest frequency modes observed in the matrix occur as a medium intensity doublet at 551.3−548.0 cm^{-1}, a weaker feature at 524.7 cm^{-1}, and a barely discernible peak at 460.1 cm^{-1}. The more intense doublet of bands has been assigned in the previous section to the Al−O stretching coordinates. In addition to the metal−ligand stretching internal coordinates, these modes are highly mixed with the benzenoid ring internal deformation modes. Closely related to these latter Al−O modes, the simulated feature at 530 cm^{-1} arises from the third Al−O vibration of this set and can be thought of as the totally symmetric Al−O stretching coordinate. Finally, the lowest frequency absorption at 460.1 cm^{-1} is attributable to a CCCC torsional motion of the ligand structure and may be associated with the simulated mode at 484 cm^{-1}.

Although $Almq_3$ is structurally very similar to Alq_3, it can be noted from Figures 2 and 3 that the infrared spectrum of $Almq_3$ is significantly more complex. Part of this added complexity arises from vibrational modes in the former complex due to the internal vibrations of the methyl groups; however, most of the spectral features due to these vibrations are expected to be very weak and are not expected to contribute significantly to the spectrum. Interestingly, the major differences between the Alq_3 and $Almq_3$ infrared spectra arise because the methyl groups in $Almq_3$ alter the natural frequencies of some of the internal modes of the quinolate ligand. These changes have caused a nearly complete redistribution of the forms of the calcu-

lated normal modes from their analogues in Alq_3, particularly those that occur below 1100 cm^{-1}. As might be expected, the normal modes that feel the least perturbation from their forms in Alq_3 are the ring C−C stretching modes. For this reason, the absorptions at 1579.9, 1574.0, and 1510.5 cm^{-1}, the broad multiplet structure at 1481.3 cm^{-1}, the doublet at 1388.4 and 1374.8 cm^{-1}, and the multiplet centered at 1321.5 cm^{-1} can all be correlated directly to their analogues in the Alq_3 spectrum. These modes are so unaffected by the addition of the methyl groups that even their profiles are similar between the two spectra.

In addition to these modes, the primarily symmetric C−N stretching modes of $Almq_3$ that occur at 1220.6 cm^{-1} show little perturbation by appearing ≈10 cm^{-1} lower in energy than the analogous mode in Alq_3. In this region of the spectrum, the only absorptions that can be directly associated with the methyl groups are the feature at 1417.3 cm^{-1} due to the CH_3 "umbrella" motion and the feature at 1246.2 cm^{-1} assigned to the aromatic ring carbon—methyl carbon (C−Me) stretching vibration. In addition, the spectral features at 1034.5 and 1014.8 cm^{-1} are associated with the methyl rocking motions.

In the spectral region below 1200 cm^{-1}, the internal angle deformation modes of the naphthalene backbone, the aromatic C−H in- and out-of-plane bending and wagging vibrations, and the CCCC torsional modes of the naphthalene backbone dominate the potential energy distributions of the normal modes. Unlike the higher frequency vibrations, the only feature that remains largely unperturbed by the methylation of the ligands occurs at 806.3 cm^{-1} (807.5 cm^{-1} of Alq_3) and can be associated with the internal angle deformations of the naphthalene skeleton. Nearly all of the other vibrations have been altered either in form or frequency from those in the parent species. For instance, the absorption in the $Almq_3$ matrix spectrum that appears at 1157.6 cm^{-1} is not a purely C−H in-plane bending vibration as in the analogous modes of Alq_3 (1119.2 and 1117.6 cm^{-1}). In $Almq_3$, these modes are significantly more mixed with contributions from the aromatic C−C stretching internal coordinates and hence exhibit a nearly 40 cm^{-1} blue shift. Similarly, the absorptions in the $Almq_3$ matrix spectrum at 895.1 and 889.4 cm^{-1} are primarily due to the aromatic CCC internal angle deformations with some contributions from the Al−N stretching coordinates. The modes closely related to these vibrations in Alq_3 produce the multiplet absorption centered at 755 cm^{-1} in the matrix spectrum of that species. By noting the spectra in Figures 2 and 3, it can be seen how the blue shift of these CCC deformation modes in $Almq_3$ has significantly simplified the spectral region around 755 cm^{-1}. In fact, only a single absorption occurs in the 750 cm^{-1} region of the $Almq_3$ matrix spectrum (744.0 cm^{-1}) and this absorption is due to the aromatic C−H out-of-plane wagging vibrations.

One of the more interesting results of the current investigation arises from the unusual mode mixing associated with the Al−O stretching modes of each complex. In $Almq_3$, these coordinates contribute significantly to the vibrations that give rise to the absorptions at 711.0, 705.8, and 692.9 cm^{-1} as well as the intense doublet at 545.6 and 542.8 cm^{-1}. The lower frequency modes display mixed character very similar in form and energy to the analogous normal modes in Alq_3 and give rise to the absorptions at 551.3 and 548.0 cm^{-1}. The higher frequency set of modes associated with the Al−O stretching coordinates present a somewhat more difficult problem. Since the calculated Al−O bond lengths in the $Almq_3$ and Alq_3 molecules are similar, one expects that the force constants of their stretching modes should be of the same magnitude. Hence, it would seem inconsistent that the Al−O stretching modes in the methylated derivative should occur 50 cm^{-1} higher in energy than the associated mode in Alq_3 unless some other factor is influencing these vibrations. The vibrations that occur in $Almq_3$ at 711.0, 705.8, and 692.9 cm^{-1} are calculated as being nearly pure Al−O stretching modes, while the analogous vibrations in Alq_3 (651.9 cm^{-1}) are severely mixed in character between the Al−O stretching coordinates and the asymmetric combination of ring breathing modes of the naphthalene fused ring system. This unusual mode mixing is the source of the apparent 50 cm^{-1} disparity between these vibrational analogues in these complexes. The asymmetric combination of the ring breathing modes in $Almq_3$ gives rise to the bands at 575.6 and 566.0 cm^{-1}, suggesting that the methyl groups have lowered the natural frequency of this internal coordinate and have decoupled it from the Al−O stretching modes.

5.4. Argon Matrix Photoluminescence Spectra of Alq_3 and $Almq_3$. The photoluminescence spectrum (PL) of Alq_3 is a broad, featureless emission centered at approximately 550 nm (510 nm for $Almq_3$) which gives Alq_3-based MOLED devices their characteristic green color. Because of the importance of this emission process, attempts to access the effects of molecular concentration in the matrix on the PL of Alq_3 and $Almq_3$ were conducted. The resultant spectra of matrix isolated Alq_3 and $Almq_3$ as a function of guest molecule concentration are shown in Figure 6 and their vibronic spectral features are listed in Table 4. Both Alq_3 and $Almq_3$ are well known for their broad green emission which remains such even in dilute liquid solutions. The present study shows that as the concentration of the metal complex in the argon matrix is reduced, it is accompanied by a blue shift in the emission. In addition, features which are attributable to a vibronic progression appear. In matrices that contain an Alq_3 mole ratio of less than 500:1, structure begins to appear on the emission band that has even energy spacings of about 13 nm or approximately 700 cm^{-1}. These data suggest that the first excited and ground electronic states are coupled by a vibrational mode that has approximately this energy.

The matrix infrared spectrum of Alq_3 has several absorptions that occur in the 700−650 cm^{-1} region that could be associated with the observed vibronic progression. Since the HOMO of Alq_3 is localized in the phenolic side of the 8-hydroxyquinoline ligand and the LUMO is localized on the pyridyl side,[21] it stands to reason that a vibrational mode that couples the two electronic states involved in this transition is localized within the "naphthalene" backbone of the ligand. The most likely candidate gives rise to the absorption at 651.9 cm^{-1}, assigned to an antisymmetric combination of ring breathing and metal−ligand stretching modes (see section 5.2). It appears that the origin of this series of transitions occurs no longer in wavelength than at about 465 nm (the highest energy feature observed in the emission spectrum), with the most probable transition occurring at 517 nm, suggesting that the transition between the upper electronic state ($\nu'(0)$ vibrational state) and the ground electronic manifold occurs by way of the $\nu(5)$ excited vibrational state of the latter normal mode. Since this transition occurs by way of such a highly excited vibrational state, there is an implication that Alq_3 undergoes a significant distortion from its ground state, equilibrium geometry as a result of electronic excitation. Calculational investigation of this effect is currently underway in our laboratory.

A similar vibronic structure appears in the $Almq_3$ PL spectrum (Figure 6). The structural features on the PL emission band of $Almq_3$ also maintain a nearly constant spacing and appear to be associated with a single vibrational mode. Unlike the spacing in Alq_3, these features are separated on the order of 600 cm^{-1}

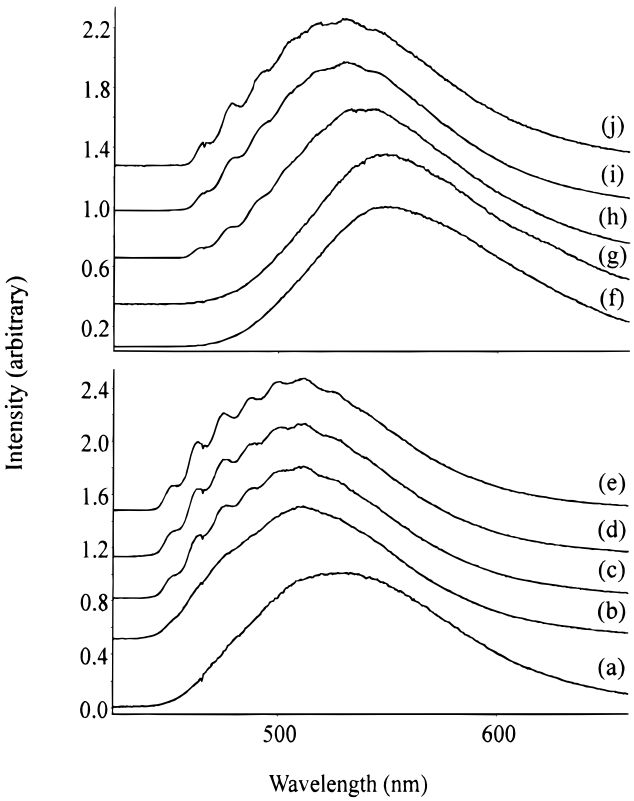

Figure 6. Photoluminescence spectra (325 nm excitation) in the 425−700 nm region of (bottom plot) $Almq_3$: (a) as a thin film, (b) 100/1 in Ar, (c) 200/1 in Ar, (d) 500/1 in Ar, (e) 7000/1 in Ar and (top plot) Alq_3 (f) as a thin film, (g) 100/1 in Ar, (h) 225/1 in Ar, (i) 500/1 in Ar, (j) 5000/1 in Ar. All spectra were collected at a substrate temperature of 11 K.

TABLE 4: Vibronic Transition Wavelengths (nm) of the $S_1 \rightarrow S_0$ Photoluminescence Transitions of Alq_3 and $Almq_3$

transition wavelength	assignment[a]
Alq_3	$\nu'(0)\rightarrow\nu(n)$
465	0→0
478	0→1
492	0→2
505	0→3
518	0→4
531	0→5
544	0→6
$Almq_3$	$\nu'(0)\rightarrow\nu(n)$
451	0→0
463	0→1
475	0→2
487	0→3
499	0→4
510	0→5
522	0→6

[a] Assignments denote transitions between vibrational quantum levels of the excited and the ground electronic states.

or about 100 cm^{-1} closer together than the analogous bands on the Alq_3 emission. Analysis of the calculated normal modes of mer-$Almq_3$ finds that the antisymmetric combination of ring breathing modes (the analogue of the mode listed above in the discussion on Alq_3) occurs in a triplet of vibrations at 586, 587, and 595 cm^{-1}. These modes can be associated with the matrix IR bands at 575.6 and 566.0 cm^{-1} which lie 76.3 and 85.9 cm^{-1} lower in energy than the analogous Alq_3 modes. Unlike the analogous vibrations in Alq_3, these modes show little contribution from the Al−O stretching which is a result of the slightly different mode mixing as mentioned above. It is interesting to note that the lack of metal ligand character in these vibrations of $Almq_3$ may explain its significantly higher photoluminescence quantum yield when compared to that of the parent molecule (0.42 for $Almq_3$ versus 0.25 for Alq_3).[11] One may speculate that the coupling of the metal−ligand stretching coordinates to this vibronic transition in Alq_3 may provide an additional path for nonradiative decay that is not available to $Almq_3$ and thus endows the latter complex with a higher photoluminescence and electroluminescence[10,12] quantum yield. Regardless, the fact that the antisymmetric combination of ring breathing modes in $Almq_3$ lies about 80 cm^{-1} below the analogous mode in Alq_3 provides further support for the assignment of the vibronic progressions observed in the fluorescence spectra of matrix isolated Alq_3 and $Almq_3$.

6. Conclusion

Matrix-isolation infrared spectroscopy and B3LYP/SDD calculations have been applied to tris(8-hydroxyquinolinato)-aluminum(III) and tris(4-methyl-8-hydroxyquinolinato)aluminum(III) in attempt to determine the relative populations of the meridional and facial isomers of each complex in the matrix environment. Hybrid DFT calculations have been applied to both the meridional and facial isomers of Alq_3 and $Almq_3$ to produce *unscaled* vibrational frequencies and normal modes that match the observed matrix-isolation infrared spectra and provide an understanding of the vibrational potential of both Alq_3 and $Almq_3$. These results also further support the remarkable predictive powers of the density functional method even for reasonably large molecular species.

By using the results of the B3LYP-based vibrational calculations in conjunction with the observed infrared spectrum, the metal−ligand stretching vibrations of both complexes have been identified and used to determine that Alq_3 and $Almq_3$ exist in primarily the meridional isomeric form. Since the meridional isomer is the primary geometric configuration of these complexes, it is obvious that any spectroscopic investigation of these materials in a device configuration (ultrathin film) will be dominated by features due to the lower symmetry isomer and as such should be interpreted with this in mind. Of further note with respect to the device applications of Alq_3 and $Almq_3$ is the fact that recent DFT investigations on the charged species have found that the $[M^+][fac\text{-}Alq_3^-]$ cation−anion pair is more stable than the associated meridional analogue.[22] This suggests that upon deposition of a metal cathode onto an Alq_3 thin film (which is the typical preparation method for MOLED devices), the resultant interface may be populated by a significant amount of the facial isomeric form. In fact, although the meridional isomer may dominate the population in the solid state, it has been found that the facial form is a better electron trap based on the relative energetics of the charged species;[21] therefore, the facial isomer (even as a significant minority in the amorphous film) may govern charge transport in the bulk material. Furthermore, as negative charge is transported through the Alq_3 thin film, isomerization between the two forms may occur as a result of charge injection at a given molecular sight. This insight comes from the fact that the energy needed for this rearrangement may be small based on NMR studies that suggest fac−mer interchange may occur rapidly in solution at temperatures as low as 100 °C.[34]

The current investigation has analyzed the effects of molecular concentration in the matrix on the photoluminescence spectra of these two species. It has been found that at low concentrations (below 500:1 Ar/analyte mole ratio), the emission bands of both complexes exhibit a vibronic progression that can be attributed

to the coupling of the vibrations of the individual ligands to the fluorescence transition. The bands observed in the PL spectra of each complex (with vibronic transitions spaced at ≈655 cm^{-1} for Alq_3 and ≈570 cm^{-1} for $Almq_3$) suggest that these transitions are coupled with a vibrational coordinate that is comprised of the asymmetric combination of the ring breathing modes of the phenolic and pyridyl sides of the quinolate ligand. The most probable transition appears to occur between the $\nu'(0)$ vibrational state in the excited electronic manifold and the $\nu(5)$ state of this normal mode in the ground electronic manifold.

Acknowledgment. The authors thank the Office of Naval Research for financial support and the Department of Defense High Performance Computing facility at the Wright-Patterson Air Force Base Aeronautical Systems Center/Major Shared Resource Center for the computing time grant. G.P.K. is a National Academy of Sciences/National Research Council postdoctoral research associate.

References and Notes

(1) Phillips, J. P. *Chem. Rev.* **1955**, *56*, 271.
(2) Stary, J. *Anal. Chim. Acta* **1963**, *28*, 132.
(3) Ballardini, R.; Varani, G.; Indelli, M. T.; Scandola, F. *Inorg. Chem.* **1986**, *25*, 3858.
(4) Hollingshead, R. G. *Oxine and Its Derivatives: Part One*; Butterworth: London, 1954.
(5) Tang, C. W.; Van Slyke, S. A. *Appl. Phys. Lett.* **1987**, *51*, 913.
(6) Forrest, S. R. *Chem. Rev.* **1997**, *97*, 1793.
(7) Tsutsui, T. *Mater. Res. Bull.* **1997**, *22*, 39.
(8) Miyata, S.; Nalwa, H. S. *Organic Electroluminescent Materials and Devices*; Gordon and Breach Publishers: Canada, 1997.
(9) Scott, J. C.; Malliaras, G. G. To appear in *Conjugated Polymers*; Hadziioannou, G., van Hutten, P., Eds.; Wiley-VCH: New York, 1999.
(10) Kido, J.; Iizumi, Y. *Chem. Lett.* **1997**, 963.
(11) Mattoussi, H.; Murata, H.; Merritt, C. D.; IIzumi, Y.; Kido, J.; Kafafi, Z. H. *J. Appl. Phys.* **1999**, *86*, 2642.
(12) Kido, J.; Matsumoto, T. *Appl. Phys. Lett.* **1998**, *73*, 20.
(13) Mori, T.; Fujikawa, H.; Tokito, S.; Taga, Y. *Appl. Phys. Lett.* **1998**, *73*, 2763.
(14) Hill, I. G.; Kahn, A. *J. Appl. Phys.* **1998**, *84*, 5583.
(15) Huang, M. B.; McDonald, K.; Keay, J. C.; Wang, Y. Q.; Rosenthal, S. J.; Weller, R. A.; Feldman, L. C. *Appl. Phys. Lett.* **1998**, *73*, 2914.
(16) Campbell, I. H.; Smith, D. L. *Appl. Phys. Lett.* **1999**, *74*, 561.
(17) Lee, S. T.; Wang, Y. M.; Hou, X. Y.; Tang, C. W. *Appl. Phys. Lett.* **1999**, *74*, 670.
(18) Schmidbaur, H.; Lettenbauer, J.; Wilkinson, D. L.; Müller, G.; Kumberger, O. *Z. Naturforsch. B* **1991**, *46B*, 901.
(19) Halls, M. D.; Aroca, R. *Can. J. Chem.* **1998**, *76*, 1730.
(20) Curioni, A.; Andreoni, W.; Treusch, R.; Himpsel, F. J.; Haskal, E.; Seidler, P.; Heske, C.; Kakar, S.; van Buuren, T.; Terminello, L. *Appl. Phys. Lett.* **1998**, *72*, 1575.
(21) Curioni, A.; Boero, M.; Andreoni, W. *Chem. Phys. Lett.* **1998**, *294*, 263.
(22) Curioni, A.; Andreoni, W. *J. Am. Chem. Soc.* **1999**, *121*, 8216.
(23) Ball, D. W.; Pong, R. G.; Kafafi, Z. H. *J. Phys. Chem.* **1994**, *98*, 10720.
(24) Ball, D. W.; Pong, R. G.; Kafafi, Z. H. *J. Am. Chem. Soc.* **1993**, *115*, 2864.
(25) Frisch, M. J.; Trucks, G. W.; Schlegel, H. B.; Scuseria, G. E.; Robb, M. A.; Cheeseman, J. R.; Zakrzewski, V. G.; Montgomery, J. A., Jr.; Stratmann, R. E.; Burant, J. C.; Dapprich, S.; Millam, J. M.; Daniels, A. D.; Kudin, K. N.; Strain, M. C.; Farkas, O.; Tomasi, J.; Barone, V.; Cossi, M.; Cammi, R.; Mennucci, B.; Pomelli, C.; Adamo, C.; Clifford, S.; Ochterski, J.; Petersson, G. A.; Ayala, P. Y.; Cui, Q.; Morokuma, K.; Malick, D. K.; Rabuck, A. D.; Raghavachari, K.; Foresman, J. B.; Cioslowski, J.; Ortiz, J. V.; Stefanov, B. B.; Liu, G.; Liashenko, A.; Piskorz, P.; Komaromi, I.; Gomperts, R.; Martin, R. L.; Fox, D. J.; Keith, T.; Al-Laham, M. A.; Peng, C. Y.; Nanayakkara, A.; Gonzalez, C.; Challacombe, M.; Gill, P. M. W.; Johnson, B.; Chen, W.; Wong, M. W.; Andres, J. L.; Gonzalez, C.; Head-Gordon, M.; Replogle, E. S.; Pople, J. A. *Gaussian 98*, rev. A.6; Gaussian Inc.: Pittsburgh, PA, 1998.
(26) Becke, A. D. *J. Chem. Phys.* **1993**, *98*, 5648.
(27) Lee, C.; Yang, W.; Parr, R. G. *Phys. Rev. B* **1988**, *37*, 785.
(28) Bergner, A.; Dolg, M.; Kuechle, W.; Stoll, H.; Preuss, H. *Mol. Phys.* **1993**, *80*, 1431.
(29) Ingel-Mann, G.; Stoll, H.; Preuss, H. *Mol. Phys.* **1988**, *65*, 1321.
(30) Dunning, T. H., Jr.; Hay, P. J. In *Modern Theoretical Chemistry*; Shaefer, H., III, Ed.; Plenum: New York, 1976; Vol. 3.
(31) Larsson, R.; Eskilsson, O. *Acta Chem. Scand.* **1968**, *22*, 1067.
(32) Pulay, P.; Fogarasi, G.; Pongor, G.; Boggs, J. E.; Vargha, A. *J. Am. Chem. Soc.* **1983**, *105*, 7037, and references therein.
(33) It must be noted that the simulated spectra are the result of fitting a sum of Lorentzian functions to the vibrational frequencies and infrared intensities produced by the B3LYP/SDD calculations. For these simulations, the calculated spectra were given a global line width of 0.50 cm^{-1} (fwhm). This is smaller than can be expected for the experimental line widths even in the matrix environment, thereby ensuring that no vibrational transitions will be obscured in the theoretical spectrum that might be resolved in the experimental one. This technique allows a more effective (and understandable) correlation between the calculated and experimentally observed spectra because a large number of the calculated normal modes for both Alq_3 and $Almq_3$ lie too close together to be resolved as individual bands in the experimental infrared spectrum (accidental degeneracy). The vibrational frequencies printed in Tables 2 and 3 are the values taken directly from the G98 output.
(34) Baker, B. C.; Sawyer, D. T. *Anal. Chem.* **1968**, *40*, 1945.